

A PROCEDURE TO DETERMINE THE CRITICAL SPEED OF RAILWAY TRACKS BASED ON THE WINKLER'S HYPOTHESIS AND STATIC FEM SIMULATIONS

JOSÉ ESTAIRE¹, INÉS CRESPO-CHACÓN¹ AND MARÍA SANTANA¹

¹Laboratorio de Geotecnia, CEDEX
Alfonso XII 3 y 5, Madrid 28014, Spain
Jose.Estaire@cedex.es, <http://www.cedex.es>

Key words: High Speed Railways, Critical Speed, FEM, Dynamic Amplification Factor, Winkler foundation, Track stiffness.

Abstract. Trains may encounter a critical speed at which the soil experiences great deformations due to large dynamic amplification of the vertical motion during train passage. In this paper, we develop a procedure, on the base of the “beam model”, to estimate the critical speed of a rail/embankment/ground system. Inter alia, the procedure requires the value of the track stiffness as an input. We take advantage of static FEM simulations to obtain this parameter. The developed procedure has been validated and applied to: (i) real measurements taken in the well-known case of Ledsgard (Sweden), and (ii) data from several tests that our research team carried out in the CEDEX Track Box facility (CTB, Spain).

1 INTRODUCTION

It was shown that trains may theoretically encounter a critical speed at which the soil experiences great deformations which could make the train derail ([1], [2] and [3]). The train speed at which the dynamic response of the railway track and its surrounding ground is intensely amplified is called the “critical speed”. This dynamic amplification occurs when the train speed reaches the surface wave velocity of the ground and is due to large vibrations that appear in the system because of a “resonance-like” condition.

Demands on high train speeds and short travel times call for straight lines, which makes, in many occasions, the crossing of soft soil zones unavoidable. Peat, organic clays and soft marine clays may have a shear wave velocity as low as 50 m/s. Therefore, problems with high-speed lines, and even traditional tracks, reaching the critical speed can be expected to an increasing amount. Unfortunately, few data from real observations and validated predictions have been reported so far in the literature.

This article shows how to take advantage of static simulations by using the two-dimensional finite element method (2D-FEM) to estimate the critical speed of a railway track. Section 2 provides a summary of the theoretical basics to estimate the critical speed of a rail/embankment/ground system on the base of a model that assumes the railway track as a beam on an elastic foundation (“beam model” hereafter). Section 3 shows the procedure to calculate the track critical speed. Section 4 is devoted to validating the previous method. Discussion, conclusions and further developments are given in Section 5.

2 BASICS: THE BEAM MODEL APPROACH

The beam model assumes that the railway track system can be replaced by an infinite elastic beam, with bending stiffness EI , resting on a viscoelastic half space, with foundation coefficient k (spring constant per unit length). The elastic foundation is assumed to be of the Winkler type, that's to say one with the foundation reaction per unit length at the horizontal position x , $p(x)$, directly proportional to the beam deflection, $z(x)$, by the factor k (Eq. 1). Let us consider that this system is loaded by a wheel load Q according to Fig. 1.

$$p(x) = kz(x) \quad (1)$$

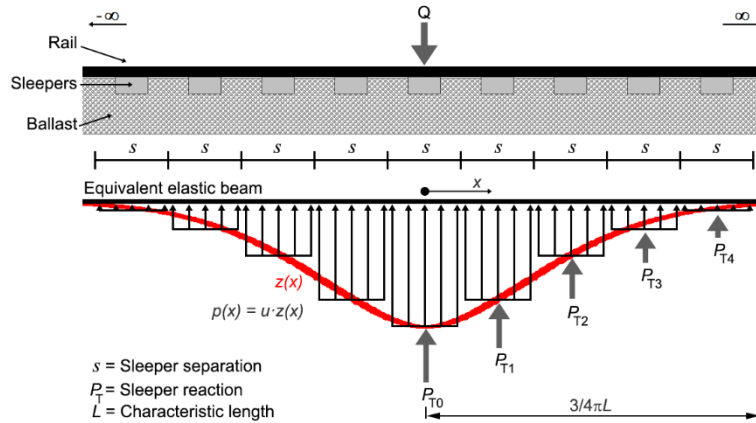


Figure 1: Infinite beam on elastic foundation model.

2.1 Static case

Assuming that Q is applied at $x = 0$, the beam deflection $z(x)$, can be calculated by using Eq. 2 [4], where L is the so-called characteristic length (Eq. 3):

$$z(x) = \frac{Q}{2kL} \left(\cos\left(\frac{|x|}{L}\right) + \sin\left(\frac{|x|}{L}\right) \right) \exp\left(-\frac{|x|}{L}\right) \quad (2)$$

$$L = \sqrt[4]{\frac{4EI}{k}} \quad (3)$$

The track stiffness (K) is defined by Eq. 4a, i.e., it is the rate between the values of a static point load (Q in this case) and the corresponding vertical rail deflection in the position in which the load is being applied (z_0). Equations 2, 3 and 4a provide Eq. 4b and 4c.

$$(a) \quad K = \frac{Q}{z_0}; \quad (b) \quad K = 2kL; \quad (c) \quad k = \sqrt[3]{\frac{K^4}{64EI}} \quad (4)$$

2.2 Quasi-static case

A detailed solution of the problem of a constant point load (Q) moving along an infinite beam (from $-\infty$ to ∞) on an elastic foundation at constant speed v (Fig. 1) is presented in this section, as developed in [5]. This problem is of great theoretical and practical significance.

In this approach the beam deflection depends not only on the position x , but also on the time t , that is $z(x,t)$. On these assumptions, $z(x,t)$ is described by Eq. 5, where: ω_N is the undamped natural frequency of the vibration ($\omega_N = (k/m)^{1/2}$ also called “track-on-ballast resonance frequency”); D is the damping ratio, i.e., the ratio between actual damping and critical damping; and m is the effective track mass per unit length (see Section 3).

$$EI \frac{\partial^4 z(x,t)}{\partial x^4} + m \frac{\partial^2 z(x,t)}{\partial t^2} + 2m\omega_N D \frac{\partial z(x,t)}{\partial t} + kz(x,t) = Q\delta(x-vt) \quad (5)$$

First, it is useful to discuss free wave propagation in the supported beam without damping, i.e. to analyze Eq. 5 with $Q = 0$ and $D = 0$. In this case, the solution can be written in the form of harmonic bending waves, $z(x,t) = A \exp(i(hx - \omega t))$, being h the wavenumber and ω the circular frequency. Under these conditions, Eq. 5 provides the following dispersion equation for track waves propagating in the system (Eq. 6):

$$\omega = \sqrt{\frac{k + h^4 EI}{m}} \quad (6)$$

From Eq. 6, the frequency-dependent phase and group velocities of track waves ($v_p = \omega/h$ and $v_g = \partial\omega/\partial h$, respectively) can be determined by expressions given in Eq. 7. Figure 2 shows the dependence of these velocities on the wavenumber for a usual high-speed line.

$$v_p = \sqrt{\frac{k + h^4 EI}{h^2 m}}; \quad v_g = \frac{2h^3 EI}{\sqrt{m(k + h^4 EI)}} \quad (7)$$

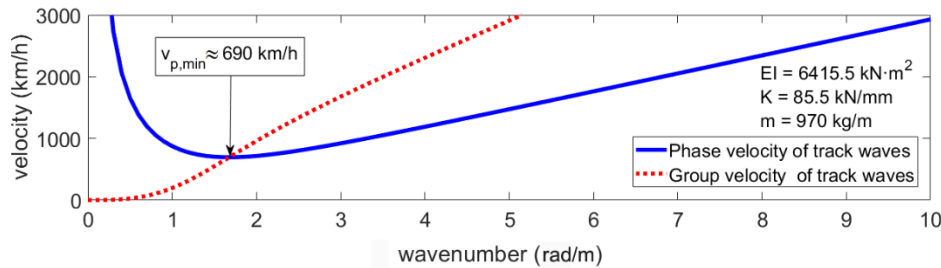


Figure 2: Phase and group velocities of track waves (in a usual high-speed line) vs. wavenumber.

The phase velocity has a minimum at $h = (k/EI)^{1/4}$, often referred as the “track critical speed”, v_{cr} (Eq. 8a). The frequency of this wave, $\omega_{v_{cr}}$, is given by Eq. 8b.

$$(a) \quad v_{cr} = v_{p,\min} = \sqrt[4]{\frac{4kEI}{m^2}}; \quad (b) \quad \omega_{v_{cr}} = \sqrt{2}\omega_N \quad (8)$$

Once discussed the free wave propagation without damping, the complete Eq. 5 is reviewed. The boundary and initial conditions for this problem are: at infinite distance to the right and to the left of force Q , the deflection, the slope of the deflection line, the bending moment and the shear force are zero for every time.

There comes into existence the so-called quasi-static state, in which the beam is at rest relative to the moving coordinate system whose origin moves together with the load at

uniform speed v . This state sets in with adequate accuracy in a comparatively short time interval after the moving force starts to act. For further discussion, it is convenient to introduce a new independent and dimensionless variable, x_{dl} , defined as $x_{dl} = (x-vt)/L$, where L is the characteristic length as given in the static case (Eq. 3).

For the quasi-static state, it can be assumed that the solution of Eq. 5 will be in the form $z(x,t) = z_0 z(x_{dl})$, being $z(x_{dl})$ the dimensionless deflection of the beam, and z_0 the static beam deflection underneath the immobile load Q (see Eq. 9, which is obtained from Eq. 3, 4a and 4b). Therefore, the quasi-static solution of Eq. 5 underneath the moving load is given by Eq. 10a. The dimensionless parameter α is the ratio of the velocity at which the load moves, v , to the track critical speed, v_{cr} (Eq. 10b); and the parameter b is the positive real root of Eq. 10c.

$$z_0 = \frac{QL^3}{8EI} \quad (9)$$

$$(a) \quad z(x_{dl} = 0) = \frac{2b}{3b^4 + 4\alpha^2 b^2 + \alpha^4 - 1}; \quad (b) \quad \alpha = \frac{v}{v_{cr}}; \quad (c) \quad b^6 + 2\alpha^2 b^4 + (\alpha^4 - 1)b^2 - \alpha^2 D^2 = 0 \quad (10)$$

Figure 3a shows the dependence of the rail deflection on the speed for different values of the damping ratio ($D = 0; 5; 10; 15; 20$; and 30%). From this plot it can be stated that the parameter v_{cr} is actually a real critical speed, in the sense that when the velocity of the load approaches that speed ($v \rightarrow v_{cr}$), the deflection amplification cannot be neglected. The lower the damping ratio, the higher the Dynamic Amplification Factor ($DAF = z/z_0$, see Fig. 3a).

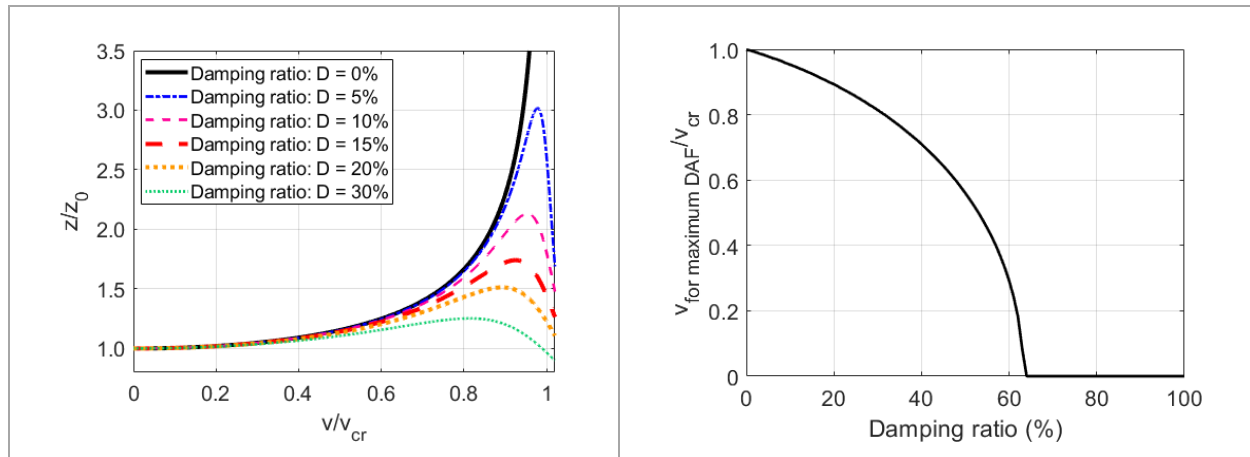


Figure 3: (a) Normalized displacement (DAF) vs. dimensionless train velocity for different damping ratios. (b) Ratio of train speed for which the DAF is maximum to critical speed vs. damping ratio.

It is worth noting that the maximum deflection takes place at $v/v_{cr} = 1$ only for damping ratio equal to zero. This implies that, in this model, the critical speed is defined as the train speed that causes infinite deflection for a null damping ratio, although for higher damping ratios the peak deflection is shifted to lower train velocities (see Fig. 3b). However, from the engineering design point of view, the situation that should be avoided in the design is the one in which the maximum deflection appears, regardless the name given to the train speed at which it occurs. The design safety factor, which is usually between 1.6 and 2.0, should therefore be applied to such velocity.

3 THE PROCEDURE TO DETERMINE THE TRACK CRITICAL SPEED

The track critical speed can be calculated by using Eq. 11, which is obtained from Eq. 8a and 4c. Therefore, the calculation of the critical speed of a railway track requires an accurate determination of EI , m and K .

$$v_{cr} = \sqrt[6]{\frac{K^2 EI}{m^3}} \quad (11)$$

a) EI : As suggested by Fortin [6], the rail is the only element that provides the bending stiffness of the beam.

b) m : The effective mass per unit of length includes the three following magnitudes¹, as suggested by Fortin [6] and corroborated in Section 4 with real data: (i) rail mass per unit of length ($m_{rail,eq}$); (ii) half of the sleeper mass per unit of length ($m_{sleeper,eq}$), which is the ratio of the half mass sleeper ($m_{sleeper}$) to the distance between the center of contiguous sleepers (s); and (iii) the mass (per unit of length) of the ballast layer that is directly loaded by the sleeper ($m_{ballast,eq}$), given by $m_{ballast,eq} = d_{ballast} \cdot H_{ballast} \cdot B_{ballast}$, where $d_{ballast}$ is the ballast density; $H_{ballast}$ is the ballast layer height; and $B_{ballast}$ can be quantified as the sleeper length over which the rail is centered. The sleeper geometry in railroad systems throughout Europe is quite similar, so in this work we assume the one used in Spain, so $B_{ballast} = 1.15$ m as seen in Fig. 4.



Figure 4: Sleeper ADIF AI-99. The red, thick line shows the length considered as $B_{ballast}$ in the procedure.

c) K : The track stiffness is calculated by using Eq. 4a. When real measurements of wheel load and its corresponding rail deflection are available for a railway line, the track stiffness can be directly obtained. However, real data are not always acquirable (e.g., during the design phase of railway tracks). In this case, the rail deflection required to calculate the track stiffness can be obtained by using FEM simulations, considering only static loading.

2D FEM simulations

Although the phenomenon under study is clearly three-dimensional, a two-dimensional model is less time consuming and easier to implement. For this purpose, we have used the PLAXIS-2D v.2015 software and worked under plain deformation conditions.

The hardening soil model with small-strain stiffness (HSSsmall hereafter) has been used to simulate the soil behavior. HSSsmall takes into account stress-dependency of stiffness moduli. This means that all stiffnesses increase with pressure. HSSsmall also accounts for the increased stiffness of soils at small strains: i.e., at low strain levels most soils exhibit higher stiffness than at engineering strain levels, and this stiffness varies non-linearly with strain.

The geotechnical parameters required by HSSsmall are: γ_{ap} = unit weight; c' = cohesion; φ' = friction angle; ψ = dilatancy angle; V_s = shear wave velocity; ν = Poisson's ratio; E_0 =

¹ Note that calculations are made considering only one rail.

Young's modulus; E_{50} = triaxial loading stiffness; E_{ur} = triaxial unloading stiffness; E_{oed} = oedometer loading stiffness; G_0 = small-strain shear modulus; and $\gamma_{0.7}$ = strain level at which the shear modulus has reduced to about 70 % of the small-strain shear modulus. The stiffness moduli and the shear modulus are derived from the shear wave velocity, the unit weight and the Poisson's ratio by using expressions given in Eq. 12.

$$E_0 = 2V_s^2 \gamma_{ap} (1+\nu); \quad E_{50} = E_0/10; \quad E_{ur} = 3E_{50}; \quad E_{oed} = E_{50}(1-\nu)/(1-\nu-2\nu^2); \quad G_0 = E_0/(2(1+\nu)) \quad (12)$$

The steps followed in the FEM simulations were:

- Step 1: Initial conditions: only the natural ground is activated, and the in-situ stresses are calculated by the K_0 method.
- Step 2: Building the railway structure: the corresponding mesh elements are activated.
- Step 3: Activation of the wheel load: the load is modelled as a uniform pressure on the whole sleeper length with value equal to the reaction of the sleeper underneath it. Thus, the role of the rail is taken into account although it is not directly included in the mesh.

The load is transferred by the rail not only to the sleeper underneath the load, but also to the neighboring sleepers. In the PLAXIS-2D models, the total load applied on the sleeper underneath the wheel is equal to the absolute value of the reaction of the sleeper underneath the load (R_{s0}). The value of R_{s0} can be easily calculated by integrating Eq. 1 in the x coordinate after replacing $z(x)$ by Eq. 2 (see Eq. 13).

$$R_{s0} = Q \left(1 - \cos \left(\frac{s}{4} \sqrt[3]{\frac{K}{EI}} \right) \exp \left(-\frac{s}{4} \sqrt[3]{\frac{K}{EI}} \right) \right) \quad (13)$$

The values of s and EI are a-priori known. Therefore, the reaction of the sleeper underneath the load depends on the track stiffness (Fig. 5).

In the FEM simulations, the Q value is the wheel load. The value of both K and R_{s0} is unknown. To calculate these two parameters, we use an iterative procedure. An initial track stiffness is assumed to calculate R_{s0} . This R_{s0} is used for the first FEM simulation to obtain z_0 . Given that R_{s0} is an increasing function of K , the sleeper reaction determined with Eq. 13 and the corresponding deflection obtained with PLAXIS-2D would be overestimated (underestimated) if K were higher (lower) than the real track stiffness. Then, K would be recalculated by replacing in Eq. 4a the obtained deflection. Note that the new K would be smaller (larger) than the previous one if the initial K were overestimated (underestimated). The new K value is used to repeat the previous steps. Iterations are performed until convergence, which is guaranteed because R_{s0} is an increasing function of K . For an experienced user, convergence is usually got in less than five iterations.

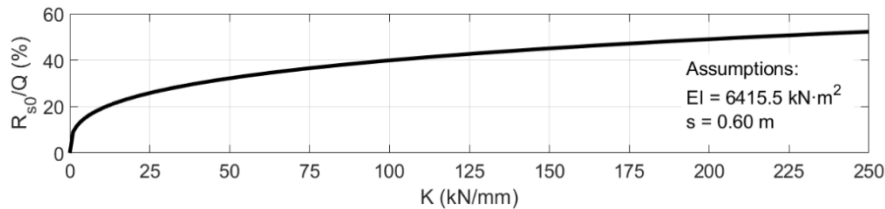


Figure 5: Sleeper reaction vs. track stiffness assuming 60 E1 type rail ($EI = 6415.5 \text{ kN}\cdot\text{m}^2$) and typical distance between sleepers ($s = 0.60 \text{ m}$). Note that for usual high-speed lines $K \approx 100 \text{ kN/mm}$ [7], so $R_{s0}/Q \approx 40 \%$.

4 VALIDATION OF THE PROCEDURE

4.1 Critical speed inferred from the DAF curves

According to Fig. 3a, if data of deflection were available for a wide range of train velocities, they could provide an estimation for the critical speed of the railway track. Thus, if vertical deflection is normalized to the static value, the critical speed will be that one that best fits the normalized data (both deflection and train speed) to DAF curves in Fig. 3a. In this way, not only the critical velocity is inferred but also the damping ratio can be estimated.

The DAF curves predicted by the beam model have been put through their paces by using data of different types: (i) measured in real tracks (Cases 1 and 2), (ii) obtained in 1:1 scale model tests (Case 3), and (iii) derived from 3D FEM dynamic calculations (Case 4). The analyzed cases are described below.

Case 1) In the frame of the so-called TGV 100 operation, measurements of the response of a real high speed track to train velocities in the range 0 – 380 km/h were collected [6]. Fig 6a shows the ratio of the measured rail deflection to the applied load in function of the train speed. Fortin [6] estimated a critical speed of 500 km/h for the instrumented track.

Case 2) At Ledsgard [8], an X-2000 passenger train was used for the tests. Its wheel load is about 87.5 kN for the locomotive and 60 kN for the rest of the cars. Figure 7a summarizes the downward and upward displacement peaks of the track from all recorded train passages, plotted versus train speed. Results from numerical simulations by Madshus and Kaynia [8] are also shown. They considered the critical speed as the train velocity at which the maximum dynamic response appeared, resulting to be 235 km/h for this site. The good agreement between the measured and simulated data provides confidence in the reliability of their physical model.

Case 3) The CEDEX Track Box (CTB, [9]) is a facility whose main objective is to test, at 1:1 scale, complete railway track sections. In the frame of research for other purposes, in October 2015 some tests were performed in CTB to analyze the effect of train speed in the global response of the track. With this aim, a special Siemens S-100 train with uniform wheel load of 79.5 kN was modelled, instead of real wheel loads (which are in the range 68.7 – 85.4 kN). The modelled train speed reached up to 400 km/h. The measured rail deflections are plotted in Fig. 8a. The deflection continuously rose with increased train speed. As no problems were detected in the railway infrastructure after the completion of the tests, the critical speed of CTB must be quite higher than 400 km/h.

Case 4) Sayeed & Shahin [10] used an advance 3D FEM model to investigate the dynamic response of a ballasted railway track-ground system to the X-2000 train moving loads at different speeds. In their model, the ballast was supported by a layered ground made of a subgrade of 7.5 m deep ($V_s = 117$ m/s) resting on hard rock. The sleeper deflection calculated for every train speed is shown in Fig 9a. The deflection peaked at 175 km/h.

The best fit of the normalized data (both deflection and train speed) to the theoretical DAF curves is plotted in Fig. 6b, 7b, 8b and 9b for the Cases 1, 2, 3 and 4, respectively. Note that the shape of the theoretical DAF curves is well matched by the data. Table 1 summarizes the results provided by these fits for both the critical speed and damping ratio. In the Cases 1 and 3 only an upper limit for the damping ratio can be estimated since the region covered by the data is not enough to discriminate between different damping ratios. The critical speed reported in the original references is also shown in Table 1, for comparison.

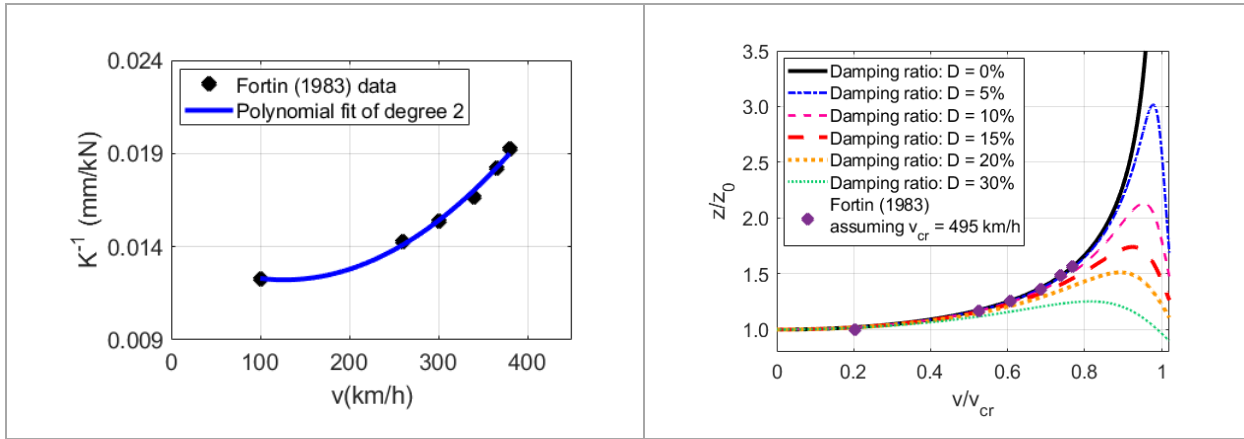


Figure 6: (a) Ratio of rail deflection to load vs. train speed for data by Fortin [6] (Case 1). (b) Normalized deflection vs. dimensionless train velocity for the data in Fig. 6a together with theoretical DAF curves.

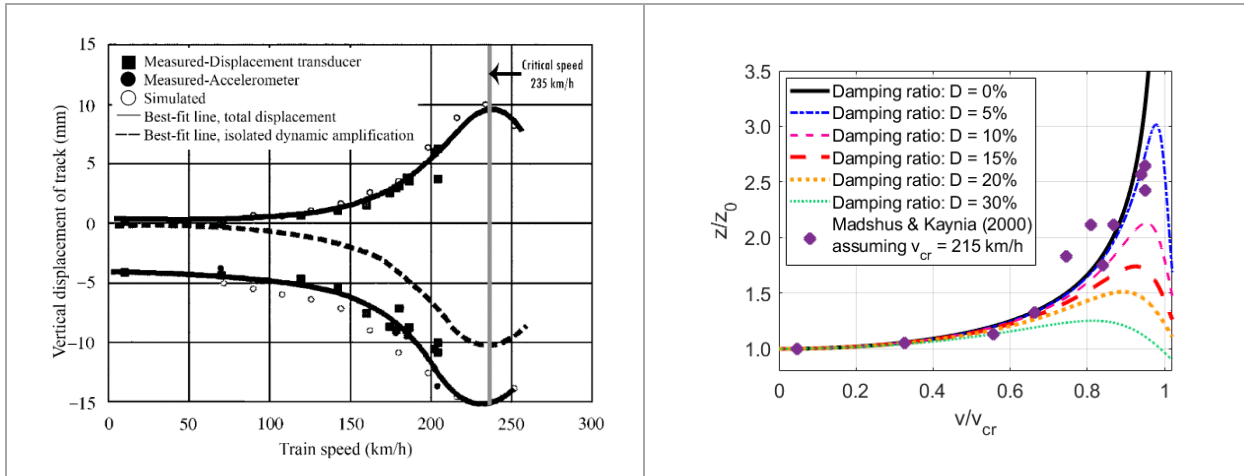


Figure 7: (a) Peak vertical displacement of the Ledsgard track (Case 2) versus train speed: measurement and simulation (adapted from [8]). (b) Normalized displacement vs. dimensionless train velocity for the real deflections shown in Fig 7a together with theoretical DAF curves.

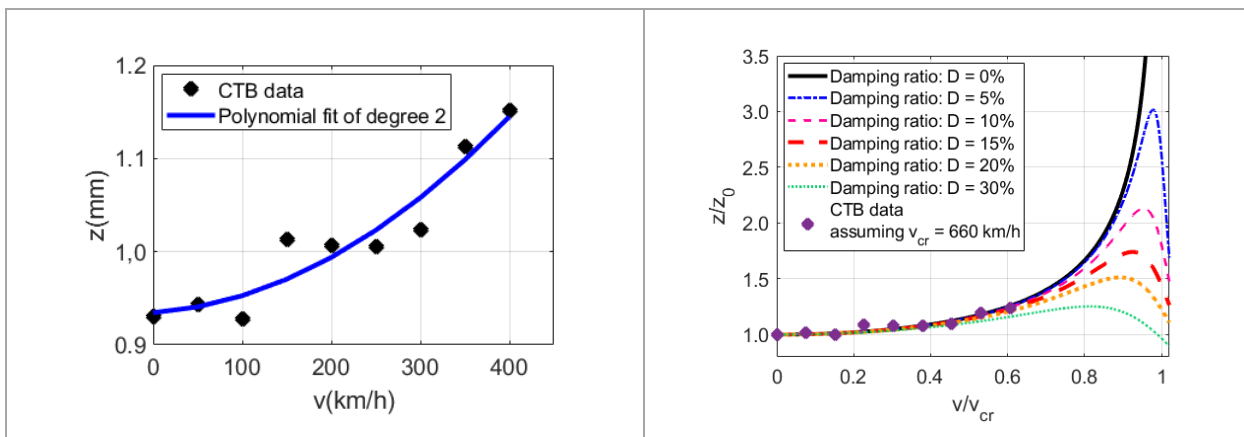


Figure 8: (a) Rail deflection vs. train speed measured at CTB (Case 3). (b) Normalized deflection vs. dimensionless train velocity for the data given in Fig. 8a together with theoretical DAF curves.

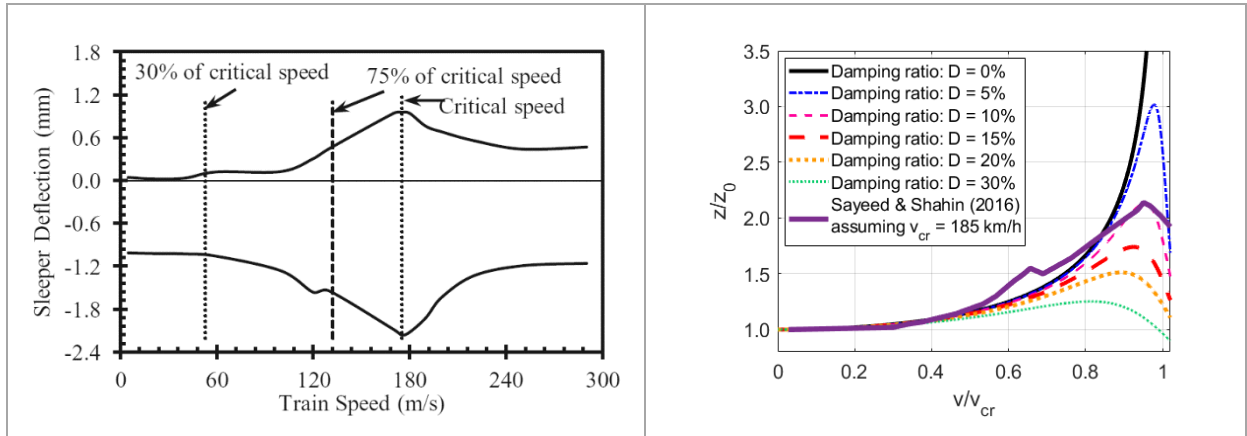


Figure 9: (a) Sleeper deflection vs. train speed for the Sayeed & Shahin [10] data (Case 4). (b) Normalized deflection vs. dimensionless train velocity for the data in Fig. 9a together with theoretical DAF curves.

Table 1: Results from fitting the original data to the theoretical DAF curves in Fig. 3a. The critical speed reported in the original reference is also shown for comparison.

	Case 1	Case 2	Case 3	Case 4
Critical speed from DAF curves (this work): v_{cr1} (km/h)	495	215	660	185
Damping ratio from DAF curves (this work): D (%)	< 10	≈ 5	< 20	≈ 10
Critical speed reported in the original reference: v_{cr2} (km/h)	500 [6]	235 [8]	>>400	175[10]
This work vs. original reference: velocity ratio v_{cr1}/v_{cr2}	0.99	0.91	----	1.06

4.2 Critical speed inferred from the procedure based on static 2D-FEM simulations

With the aim of checking the validity of the developed procedure (Section 3), we have applied it to the Cases 2 (Ledsgard) and 3 (CTB). These cases have been chosen for this purpose since they are the only ones that simultaneously satisfy the following conditions: (i) to involve real measurements, and (ii) both the geometry of the site and the geotechnical parameters are known, allowing FEM simulations to be performed.

As the wheel load and the static rail deflection are known for Ledsgard and CTB, the track stiffness can be directly calculated (Eq. 4a) and the critical speed can be estimated by using the input data in Table 2 and Eq. 11. Results are shown in Table 2.

Nevertheless, if rail deflections were not available, the FEM simulations described in Section 3 should be performed to calculate the rail deflection and the corresponding track stiffness. The geometry for the PLAXIS models of the Ledsgard site and CTB facility has been taken from [8] and [9], respectively. The phreatic level has been situated at the ground surface for the Ledsgard model and at the bottom for the CTB model. The geotechnical parameters are listed in Table 3 for Ledsgard and Table 4 for CTB. Triangular elements of 15 nodes have been used. More details about the FEM simulations are reported in [11]. Figure 10a shows the mesh for Ledsgard. Figure. 10b shows the results from FEM simulations by PLAXIS for Ledsgard for both the locomotive and a typical wagon of an X-2000 train.

Results from applying this procedure are given in Table 2. Note that the track stiffness obtained by taking advantage of the described FEM simulations is very similar to the one

inferred from real rail deflections. They differ by 2 – 3 kN/mm in the soft case (Ledsgard) and 6 kN/mm in the stiff case (CTB). This provides confidence in the reliability of 2D FEM simulations and the hypotheses that have been made for studying this kind of problems.

The critical speed obtained with the developed procedure for the Ledsgard case is in the range 229 – 242 km/h. These values are in good agreement with the one reported by Madhus & Kaynia [8]: 235 km/h. They differ less than 7 km/h (3 %).

The critical speed inferred for the CTB case from FEM simulations is 674 km/h, only 3 % lower than the value obtained when using the measured static deflection (692 km/h).

When the normalized displacement - velocity relationships (DAF curves) are used to obtain critical speeds, the results seems to be only about 15 – 30 km/h lower than those inferred from the developed procedure, regardless of the absolute value of the critical speed.

Since the results obtained with the developed method agree with those reported by other authors and/or methods, it can be concluded that the procedure, under the assumptions described in Section 3, provides reliable values for the critical speed of railway tracks.

Table 2: Input data to calculate the critical speed for Ledsgard (Case 2) and CTB (Case 3), and results obtained by using the developed procedure.

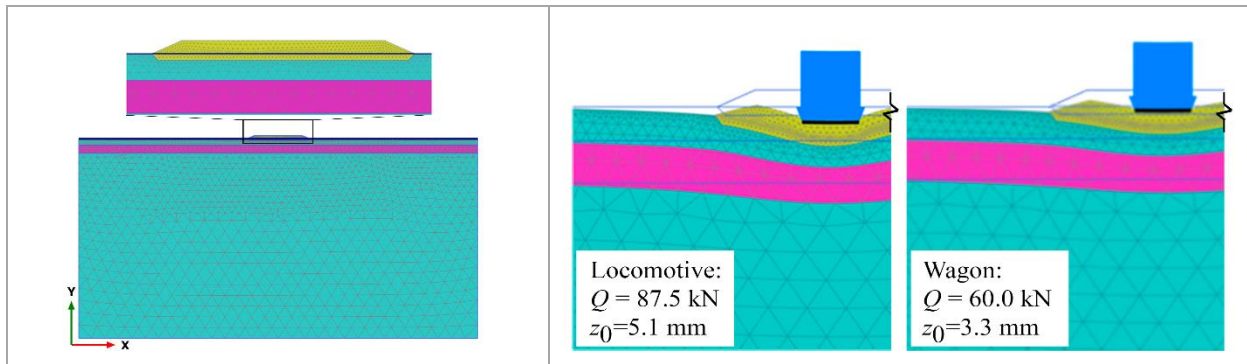
<i>Input data</i>			
	Ledsgard case		CTB tests
EI (kN·m ²)	6415.5 (60 E1 type rail)		6415.5 (60 E1 type rail)
$m_{\text{rail,eff}}$ (kg/m)	60		60
s (m)	0.67		0.60
m_{sleeper} (kg)	325		325
B_{ballast} (m)	1.15		1.15
H_{ballast} (m)	1.20		0.35
d_{ballast} (kg/m ³)	1800		1600
	Locomotive	Wagon	
Q (kN)	87.5	60	79.5
z_0 (mm)	5.7	4.0	0.93
<i>Results for masses per unit length</i>			
	Ledsgard case		CTB tests
$m_{\text{sleeper,eff}}$ (kN·s ² /m ²)	0.24		0.27
$m_{\text{ballast,eff}}$ (kN·s ² /m ²)	2.48		0.64
m (kN·s ² /m ²)	2.79		0.97
<i>Results for track stiffness and critical speed from measured deflections (z_0)</i>			
	Ledsgard case		CTB tests
	Locomotive	Wagon	
K (kN/mm)	15	15	85
v_{cr} (km/h)	231	229	692
$\omega_{v_{\text{cr}}}$ (rad/s)	61	60	322
<i>Results for track stiffness and critical speed from FEM calculations (i.e., assuming unknown z_0)</i>			
	Ledsgard case		CTB tests
	Locomotive	Wagon	
z_0 (mm)	5.1	3.4	1,01
K (kN/mm)	17	18	79
v_{cr} (km/h)	239	242	674
$\omega_{v_{\text{cr}}}$ (rad/s)	65	67	306

Table 3: Geotechnical parameters used in FEM calculations for Ledsgard.

Layer	γ_{ap} (kN/m ³)	c' (kN/m ²)	ϕ' (°)	ψ (°)	V_s (m/s)	ν	$\gamma_{0.7}$
Embankment	18	20	35	0	250	0.25	$2 \cdot 10^{-4}$
Crust	15	60	0	0	60	0.40	$10 \cdot 10^{-4}$
Organic clay	15	30	0	0	45	0.45	$20 \cdot 10^{-4}$
Clay	16	60	0	0	60	0.40	$20 \cdot 10^{-4}$

Table 4: Geotechnical parameters used in FEM calculations for CTB.

Layer	γ_{ap} (kN/m ³)	c' (kN/m ²)	ϕ' (°)	ψ (°)	V_s (m/s)	ν	$\gamma_{0.7}$
Ballast	16	20	50	20	350	0.20	$3.5 \cdot 10^{-5}$
Subballast	23	10	40	10	300	0.30	$3.5 \cdot 10^{-5}$
Form layer	22	20	35	5	250	0.30	$16.0 \cdot 10^{-5}$
Embankment	20	20	30	0	200	0.30	$22.0 \cdot 10^{-5}$


Figure 10: (a) Mesh for the FEM model of the Ledsgard site. (b) PLAXIS results for the locomotive (left) and a wagon (right) loads at Ledsgard site. In Fig 10b, the deformed mesh is scaled up 300 times.

5 DISCUSSION, CONCLUSIONS AND FURTHER DEVELOPMENTS

- The theoretical DAF curves provide a reliable value for the critical speed when they are used to fit data of rail deflection vs. train speed, regardless of the source of deflections: measured in real tracks, 1:1 scale model tests, or from FEM dynamic calculations.
- The beam model has been proved to be a simple but powerful tool to estimate the critical speed of railway tracks. It works from low to high track stiffnesses. It only needs three features of the track (see Eq. 11): (i) rail bending stiffness; (ii) effective mass per unit length; and (iii) track stiffness. Note that the theoretical DAF curves from the beam model can also be used to calculate the critical speed without making use of any of these parameters. This provides more confidence on the results obtained by using the DAF curves than on those inferred from Eq. 11. Unfortunately, the DAF curves require measurements in a wide range of train speeds, which are usually not available.
- We have corroborated the following Fortin's suggestions [6]: (i) the rail is the only element that provides the bending stiffness of the beam; and (ii) the only elements that contribute to the effective track mass are the rail, the sleeper, and a specific region of the ballast layer that has been quantified in our procedure. In this regard, it is worth noting that the real

value of the effective track mass is hard to determine, so the dependency of the “beam model” on this parameter complicates its implementation.

- 2D FEM static simulations have been demonstrated to give reliable values for the track stiffness to be used in the critical speed calculations whenever direct measurements for wheel loads and rail deflections are not available.

In addition to the “beam model” (this paper), it must be highlighted that the so-called “SASW model” [12] is another approach to calculate the critical speed. The “SASW model” is based on the dispersion curve of surface waves. While the “beam model” consists on a bending wave problem, the “SASW model” considers the critical speed to be the velocity of a surface wave with a frequency nearly equal to the carriage passage frequency.

The “SASW model” is considered to be more appropriate to infer the critical velocity since the ground mechanical parameters involved in this model (mainly the shear wave velocity) better represent the physical phenomenon under study, i.e., the interaction between the effect of moving loads in the underneath ground and the waves generated in it. Besides, the “SASW model” is quite easy to implement and does not need any further interpretation.

REFERENCES

- [1] Frýba, L. 1973. *Vibrations of solids and structures under moving loads*. Noordhoff International Publishing. Groningen, ISBN 90 01, 48p.
- [2] Debarros, F. C. P. & Luco, J. E. 1994. Response of a layered viscoelastic half-space to a moving point load. *Wave Motion* 19: 189-210.
- [3] Krylov, V.V. 1995. Generation of ground vibrations by superfast trains. *Appl. Acoust.* 44: 149-164.
- [4] Zimmermann, H. 1888. *Die Berechnung des Eisenbahnoberbaus*: Verlag, Ernst & Sohn.
- [5] Krylov, V. V. 2001. Generation of ground vibration boom by high-speed trains. *Noise and vibration from High-Speed Trains*. Thomas Telford Publishing: 251-283.
- [6] Fortin, J. P. 1983. Dynamic track deformation. *French Railway Review*, Vol. 1,1: 3-12.
- [7] Estaire, J., García-de-la-Oliva, J. L. & Crespo-Chacón, I. 2019 (In preparation). Measurements of train loads and sleeper reactions in high-speed railway lines. In *Proceedings of the XVII European Conference on Soil Mechanics and Geotechnical Engineering*. Reykjavik.
- [8] Madshus, C. & Kaynia, A. M. 2000. High-speed railway lines on soft ground: dynamic behaviour at critical train speed. *J. Sound Vibration* 231(3): 689-701.
- [9] Estaire, J., Cuéllar, V. & Santana, M. 2017. Testing railway tracks at 1:1 scale at CEDEX Track Box. In *Proceedings of the Intern. Cong. on High-Speed Rail. Technologies and Long Term Impacts*. Ciudad Real.
- [10] Sayeed, M.A. & Shahin, M. 2016, Investigation into Impact of Train Speed for Behavior of Ballasted Railway Track Foundations. In *Advances in Transportation Geotechnics 3: The 3rd International Conference on Transportation Geotechnics*. Guimarães.
- [11] Estaire, J. & Crespo-Chacón, I. 2018 (In press). Determining the railway critical speed by using static FEM calculations. In *Proceedings of the 9th European Conference on Numerical Methods in Geotechnical Engineering*. Porto.
- [12] Estaire, J., Pita, M. & Santana M. 2018 (In preparation). Determination of the critical speed of railway tracks based on the Spectral Analysis of Surface.